

Panglossian Prospects for Detecting Neutralino Dark Matter in Light of Natural Priors?

Benjamin C. Allanach¹ and Dan Hooper^{2,3}

¹ *DAMTP, CMS, University of Cambridge, Wilberforce Road, Cambridge, CB3 0WA, UK*

² *Fermi National Accelerator Laboratory, Theoretical Astrophysics, Batavia, IL 60510, USA*

³ *The University of Chicago, Department of Astronomy and Astrophysics, Chicago, IL 60637, USA*

ABSTRACT: In most global fits of the constrained minimal supersymmetric model (CMSSM) to indirect data, the *a priori* likelihoods of any two points in $\tan\beta$ are treated as equal, and the more fundamental μ and B Higgs potential parameters are fixed by potential minimization conditions. We find that, if instead a flat (“natural”) prior measure on μ and B is placed, a strong preference exists for the focus point region from fits to particle physics and cosmological data. In particular, we find that the lightest neutralino is strongly favored to be a mixed bino-higgsino ($\sim 10\%$ higgsino). Such mixed neutralinos have large elastic scattering cross sections with nuclei, leading to extremely promising prospects for both underground direct detection experiments and neutrino telescopes. In particular, the majority of the posterior probability distribution falls within parameter space within an order of magnitude of current direct detection constraints. Furthermore, neutralino annihilations in the sun are predicted to generate thousands of neutrino induced muon events per years at IceCube. Thus, assuming the framework of the CMSSM and using the natural prior measure, modulo caveats regarding astrophysical uncertainties, we are likely to be living in a world with good prospects for the direct and indirect detection of neutralino dark matter.

KEYWORDS: Supersymmetry, Effective Theories, Cosmology of Theories Beyond the Standard Model, Dark Matter.

Contents

1. Introduction	1
2. The Measure of CMSSM Parameter Space	2
3. Electroweak Symmetry Breaking and CMSSM Parameter Space	5
4. Direct Detection	11
5. Indirect Detection	13
5.1 Neutrino Telescopes	13
5.2 Gamma-Rays and Charged Particles	17
6. Summary and Conclusions	19

1. Introduction

For a variety of reasons, supersymmetry is considered to be among the most attractive extensions of the Standard Model. In particular, weak-scale supersymmetry provides an elegant solution to the hierarchy problem [1], and enables grand unification by causing the gauge couplings of the Standard Model to evolve to a common scale [2]. From the standpoint of providing a dark matter candidate, the lightest neutralino is naturally stable by virtue of R-parity conservation [3], and in many models is thermally produced in the early universe in a quantity similar to the measured density of cold dark matter [4].

In addition to collider searches for superpartners, a wide range of astrophysical experiments are currently operating and being developed in the hopes of detecting neutralino dark matter [5]. These techniques can be classified as direct and indirect detection. While the former efforts are designed to observe the elastic scattering of neutralinos with target nuclei, the latter techniques attempt to detect the annihilation products of neutralinos, including gamma-rays [6], neutrinos [7], positrons [8], antiprotons [9], antideuterons [10], and synchrotron radiation [11]. In addition to astrophysical inputs, the prospects for direct and indirect dark matter detection depend on the mass and couplings of the lightest neutralino, and in turn on the many parameters which define the masses and couplings of the superpartners.

Weak-scale supersymmetry could take a great variety of forms, depending on the details of how supersymmetry is broken. Empirically, our insights into this question are limited to the measurements of observables indirectly related to the supersymmetric spectrum, such as the anomalous magnetic moment of the muon, the $b \rightarrow s\gamma$ branching fraction, the $B_s \rightarrow \mu^+\mu^-$ branching fraction, the mass of the W boson, the effective leptonic mixing angle, Higgs boson and sparticle search constraints, and the cosmological dark matter abundance. Such observables have been used in the past to constrain the properties of the CMSSM spectrum (see, for example, Refs. [12, 13, 14, 15, 16]). Ultimately, this information can be used to determine the posterior probability distribution over the parameter space of supersymmetry. In Refs. [17, 18, 19], it was used to examine the prospects for dark matter detection.

In this paper, we consider another input that can play a significant role in determining the posterior distribution over supersymmetric parameters. In particular, we consider the measure which is associated with each point in parameter space and define a prior measure which is flat in terms of fundamental CMSSM parameters. In our analysis, we closely follow Ref. [16], but focus on the phenomenology of neutralino dark matter in the regions of supersymmetric parameter space favored by indirect constraints *and* naturalness considerations. When a natural prior measure (flat in more fundamental CMSSM parameters, rather than in $\tan\beta$) is included in the analysis of the parameter space of the constrained minimal supersymmetric standard model (CMSSM), we find that the focus point region is highly preferred. In this region, the lightest neutralino χ_1^0 is a mixed bino-higgsino ($\sim 10\%$ higgsino fraction) and, therefore, has relatively significant couplings to the Standard Model.

The prospects for the direct and indirect detection of neutralino dark matter in the favored regions are highly promising. In particular, about 61% of the posterior probability distribution predicts a neutralino-nucleon elastic scattering cross section of $\sigma_{\chi^0 N} \approx 10^{-8} - 10^{-7}$ pb, which is within one order of magnitude of the current direct detection constraints. The remaining 35% of the posterior probability distribution corresponds to parameter space in which the lightest neutralino has somewhat smaller couplings (and direct detection rates) but still annihilates efficiently in the early universe via the light Higgs resonance ($2m_{\chi^0} \approx m_h$). The projected rates at neutrino telescopes are also extremely promising, with most of the posterior probability distribution being made up of models which predict thousands of events per year at a kilometer-scale neutrino telescope such as IceCube. Current constraints from Super-Kamiokande and Amanda/IceCube already exclude a sizable fraction of the otherwise favored probability distribution. We also discuss the prospects for indirect detection using gamma-rays and charged cosmic ray particles.

2. The Measure of CMSSM Parameter Space

The CMSSM parameter space consists of the following supersymmetry (SUSY) break-

ing parameters: the universal scalar mass m_0 , the universal gaugino mass $m_{1/2}$, and the universal tri-linear scalar coupling A_0 . These parameters constrain the SUSY breaking terms in the CMSSM potential at a high energy scale, which is usually taken to be M_{GUT} , the scale at which the electroweak gauge couplings unify. In addition, $\tan\beta$ is often used to characterize the ratio of the two Higgs doublet vacuum expectation values and is taken to be an input parameter. When performing global fits to the CMSSM, it is important to take into account any smearing due to variations in important Standard Model input parameters, which we denote collectively as s . One defines the likelihood, $p(D, M_Z^{emp}|m_0, m_{1/2}, A_0, \tan\beta, s, M_Z)$, by calculating the probability density of the parameter point reproducing all current data, D . We have singled out the empirically measured Z^0 boson pole mass, M_Z^{emp} , and the one predicted in the CMSSM, M_Z , since they have a special rôle in what follows.

Here in contrast, in order to make probabilistic inferences, we begin by defining a measure in the parameter space of the CMSSM by following Ref. [16]:

$$p(D) = \int d\mu dB dA_0 dm_0 dm_{1/2} ds [p(m_0, m_{1/2}, A_0, \mu, B, s) p(D, M_Z^{emp}|m_0, m_{1/2}, A_0, \mu, B, s)], \quad (2.1)$$

where $p(m_0, m_{1/2}, A_0, B, \mu, s)$ is the joint prior probability distribution for CMSSM and Standard Model parameters. In fact, M_Z and $\tan\beta$ are related to the more fundamental parameters by the MSSM Higgs potential minimization conditions [20]:

$$\mu^2 = \frac{\bar{m}_{H_1}^2 - \bar{m}_{H_2}^2 \tan^2\beta}{\tan^2\beta - 1} - \frac{M_Z^2}{2} \quad (2.2)$$

$$\mu B = \frac{\sin 2\beta}{2}(\bar{m}_{H_1}^2 + \bar{m}_{H_2}^2 + 2\mu^2). \quad (2.3)$$

Eq. 2.2 is applied at a renormalization scale equal to the geometric mean of the two stop masses, $Q \sim \sqrt{m_{\bar{t}_1} m_{\bar{t}_2}}$, which cancels some larger logarithms in higher order corrections and results in higher accuracy. $\bar{m}_{H_1}^2$ and $\bar{m}_{H_2}^2$ are obtained from the universality boundary condition on scalar masses at M_{GUT} . They are run to Q and corrected by some tadpole loop corrections [21]. Since M_Z^{emp} and the other data, D , are independent,

$$p(D, M_Z^{emp}|m_0, m_{1/2}, A_0, \tan\beta, s) = p(D|m_0, m_{1/2}, A_0, \tan\beta, s) \times p(M_Z^{emp}|m_0, m_{1/2}, A_0, \tan\beta, s). \quad (2.4)$$

Direct current data imply that the Z^0 boson mass is extremely well constrained, $M_Z^{emp} = 91.1876 \pm 0.0021$ [22], and so we make the approximation:

$$p(M_Z^{emp}|m_0, m_{1/2}, A_0, \tan\beta, s) \approx \delta(M_Z - M_Z^{emp}). \quad (2.5)$$

In the present paper, $p(m_0, m_{1/2}, A_0, \mu, B, s)$ is defined to be a constant, resulting in so-called ‘‘flat’’ priors in the named parameters. Probabilistic inferences may be

made based upon the *posterior* probability distribution, defined to be the product of likelihood and prior, integrated over all parameters except for the ones we are interested in, using the previously defined measure. In most previous Bayesian global fits to the CMSSM [14, 17, 18, 19, 23, 24], (often flat) prior probability distributions were defined in terms of the measure

$$dM \equiv d \tan \beta dM_Z dm_0 dm_{1/2} dA_0 ds. \quad (2.6)$$

We refer to dM as the “flat $\tan \beta$ ” measure if it is used in conjunction with a prior probability distribution that is flat in each of the parameters named on the right-hand side of Eq. 2.6. One must be aware that different measures for the parameters may be chosen, and will affect the results if the power of the data is weak. For example, in Ref. [23], dM priors that were flat in $\ln m_0$ and $\ln m_{1/2}$ were compared to those that are flat in m_0 and $m_{1/2}$. In Ref. [24], a naturalness prior was introduced in terms of dM that disfavors regions of parameter space for which large cancellations are necessary in the Higgs potential [25]. In Ref. [16], $p(m_0, m_{1/2}, A_0, \mu, B, s)$ from Eq. 2.1 was chosen to strongly disfavor hierarchies between the different parameters, encoding the prejudice that they should be of the same order. In this study, we drop the “of the same order” prejudice, which was deemed by Ref. [18] to be going a step too far. By comparing the results found in studies using different prior measures, some non-negligible dependence upon the prior measure chosen can be found, indicating that determinations of the favored regions of the CMSSM parameter space from current data are somewhat uncertain. If more data compatible with the CMSSM is obtained in the future, it is expected that this unwanted dependence on the choice of the prior measure will be reduced.

Following Ref. [16]¹, substituting Eqs. 2.5 and 2.4 into Eq. 2.1, and calculating the Jacobian of $d\mu dB \rightarrow d \tan \beta dM_Z$ from Eqs. 2.2 and 2.3, we arrive at a map between dM and our desired measure:

$$p(D) = \int d \tan \beta dA_0 dm_0 dm_{1/2} ds [p(m_0, m_{1/2}, A_0, \mu, B, s) p(D|m_0, m_{1/2}, A_0, \mu, B, s) M_Z \left| \frac{B \tan^2 \beta - 1}{\mu \tan \beta \tan^2 \beta + 1} \right| \Big]_{M_Z=M_Z^{emp}}, \quad (2.7)$$

where μ and B are obtained from Eqs. 2.2 and 2.3. For now, until more data are obtained, we are stuck with dependence upon the priors and so attempts to make good guesses for reasonable prior distributions are important. The prior measure defined in Eq. 2.7 is clearly superior to dM because it is phrased in terms of parameters that are more fundamental to the model: namely, μ and B rather than $\tan \beta$ and M_Z . We shall compare and contrast the posterior samples obtained from these

¹Note that in Ref. [16], the prior factor in Eq. 2.7 was called the “REWSB” prior. Here, we refer to it as a “natural prior”.

different priors. Note that one can still argue whether the prior measure should be flat in μ and B , or whether some other measure (such as one flat in $\log B$ and $\log \mu$ for instance, see the discussion in Ref. [16]) is more appropriate. If a flat prior in $\log B$, $\log \mu$ is taken, one can multiply the integrand of Eq. 2.7 by a further factor of $1/(B\mu)$. Whichever choice is taken, we believe that the connection with the fundamental parameters of the MSSM is clearer if one starts from a measure $d\mu dB$, rather than $d\tan\beta dM_Z$. We refer to the prior measure defined in Eq. 2.7 with constant $p(m_0, m_{1/2}, A_0, \mu, B, s)$, as the natural prior.

3. Electroweak Symmetry Breaking and CMSSM Parameter Space

Our calculation of the likelihood closely follows the calculation found in Ref. [16], with additional b -physics observables and updated empirical values. The four important Standard Model (SM) inputs referred to in the previous section collectively as s are: the inverse fine structure constant evaluated in the \overline{MS} scheme at M_Z , $1/\alpha^{\overline{MS}}(M_Z) = 127.918 \pm 0.018$ [22], the equivalent version of the strong coupling constant, $\alpha_s^{\overline{MS}}(M_Z) = 0.1176 \pm 0.002$ [22], the bottom quark mass evaluated at its own mass, $m_b(m_b)^{\overline{MS}} = 4.20 \pm 0.07$ GeV [22], and the pole top quark mass, $m_t = 172.6 \pm 1.8$ GeV [26]. The muon decay constant is very accurately determined, and its central value is used as a fixed input, $G_\mu = 1.16637 \times 10^{-5}$ GeV $^{-2}$, and is used to predict the W boson pole mass, M_W .

Observable	Central value	Combined Uncertainty	References
$R_{BR(B_u \rightarrow \tau\nu)}$	1.259	0.378	[27]
Δ_{o-}	0.0375	0.0289	[28]
$R_{\Delta_{m_s}}$	0.85	0.12	[27, 29]
$\delta a_\mu \times 10^{10}$	29.5	8.8	[30]
M_W	80.398 GeV	27 MeV	[31]
$\sin^2 \theta_w^l$	0.23149	0.000173	[32, 33]
$BR(b \rightarrow s\gamma) \times 10^4$	3.55	0.72	[34]
$\Omega_{DM} h^2$	0.1143	0.01	[4]

Table 1: Indirect constraints used. For each quantity, an estimate of the theoretical error in our CMSSM prediction has been added to the empirical error in quadrature.

In table 1, we show the updated values of the observables used in our likelihood calculation, along with the relevant references. Here, $R_{BR(B_u \rightarrow \tau\nu)}$ is the ratio of the experimental and SM predictions of the branching ratio of B_u mesons decaying into a tau and a tau neutrino. The SM prediction of this quantity is rather uncertain because of two incompatible empirically derived values of $|V_{ub}|$: $(3.68 \pm 0.14) \times 10^{-3}$ versus the value coming from inclusive semi-leptonic decays, $(4.49 \pm 0.33) \times 10^{-3}$.

We simply combine these two measurements assuming independent Gaussian errors to give our SM prediction of the branching ratio $BR^{\text{SM}}(B_u \rightarrow \tau\nu) = (112 \pm 25) \times 10^{-6}$. $R_{\Delta_{m_s}}$ is the ratio of the experimental and the SM neutral B_s meson mixing amplitudes. Δ_{0-} is the isospin asymmetry in $B \rightarrow K^*\gamma$ decays.

We have used `SOFTSUSY2.0.17` [21] to calculate the sparticle and Higgs masses and couplings. Any point in the CMSSM parameter space contravening 95% confidence level sparticle direct search limits is given zero likelihood as described in Ref. [23]. The SM inference of the LEP2 Higgs search may be used to constrain the lightest CP-even Higgs boson h^0 of the CMSSM, since other constraints force the model to be in the decoupling SM-like régime. Thus, likelihood penalties from LEP2 are combined with a 3 GeV Gaussian smearing to model the uncertainty in the `SOFTSUSY2.0.17` theoretical prediction. The SUSY Les Houches Accord [35] is used to transfer the spectral information to `micrOMEGAs2.1` [36], which calculates the relic density of neutralino dark matter and its elastic scattering and annihilation cross sections, and `SuperIso2.0` [38], which calculates the branching ratio of b quarks into s quarks and a photon using one-loop MSSM corrections and NNLO SM QCD corrections. `SuperIso2.0` is also used to predict Δ_{0-} . M_W and $\sin^2\theta_w^l$ are predicted with the full two-loop MSSM effects included [39]. $R_{\Delta_{m_s}}$ and $R_{BR(B_u \rightarrow \tau\nu)}$ are computed using the approximate one-loop expressions in Refs. [40, 41] respectively.

We performed a Markov Chain Monte Carlo bank sampling scans [42] over four SM inputs and the four continuous CMSSM parameters, choosing $\mu > 0$. There is a statistical preference coming from the $(g-2)_\mu$ measurement [23]. Several chains were run using different random numbers for 200,000 steps each. For each chain, 5000 bank points were obtained at random from previous $10 \times 50,000$ step scouting Metropolis runs. In particular, it was important to include points from the h -pole region, the stau co-annihilation region and the focus point region in the bank (all described below) as these good-fit regions were (in some cases) not simply connected, a situation ideally suited to bank sampling. Enough chains were generated in order that they satisfy the Gelman and Rubin convergence criterion of $\sqrt{\hat{R}} < 1.05$ [43]. $\sqrt{\hat{R}}$ provides an estimated upper bound on the decrease in standard deviation that could be obtained in any of the eight input parameters by running the MCMC chains for more steps. 9 chains were sufficient for natural priors, whereas 20 were sufficient for the flat prior case. Our scan was performed over the parameter ranges: $60 \text{ GeV} < m_{1/2} < 2 \text{ TeV}$, $60 \text{ GeV} < m_0 < 4 \text{ TeV}$, $-4 \text{ TeV} < A_0 < 4 \text{ TeV}$, $2 < \tan\beta < 62$. Bank sampling allows us to efficiently sample from distributions which have well separated peaks, which is the case for the natural posterior probability distribution.

In Fig. 1, we show the posterior probability distribution marginalized to three dimensions, m_0 , $m_{1/2}$ and $\tan\beta$, resulting from the fit. The darker inner surface contains 68% of the probability distribution and the outer lighter surface contains 95%. In Fig. 2, we show the same distribution, marginalized to two dimensions (m_0

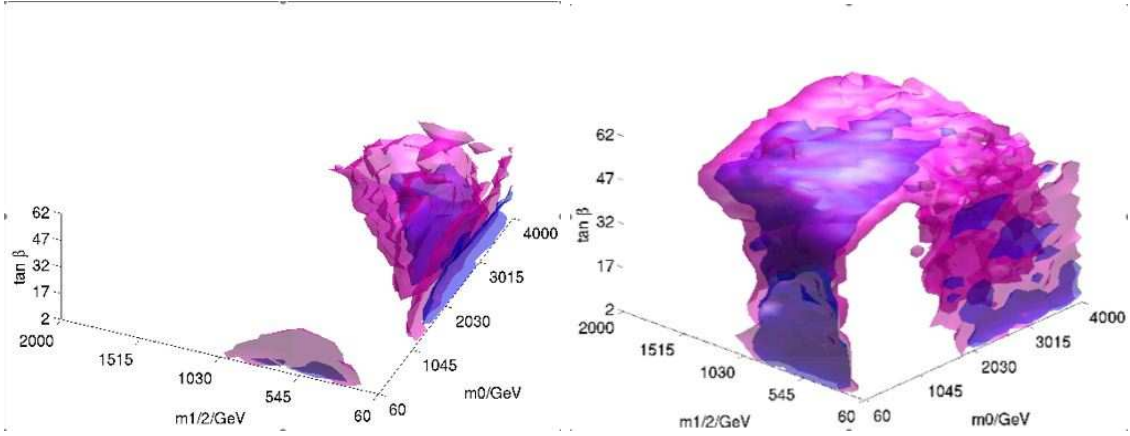


Figure 1: Iso-posterior probability density surfaces of the CMSSM parameters, projected in three dimensions. The posterior has been marginalized over the unseen parameters, taking into account the empirical inputs described in the text and using a natural prior (left) or the flat $\tan\beta$ prior (right) as described in the text. The inner (outer) surfaces contain 68%(95%) of the posterior probability density, respectively. The natural prior enhances the focus point region (bottom) for the reasons discussed in the text.

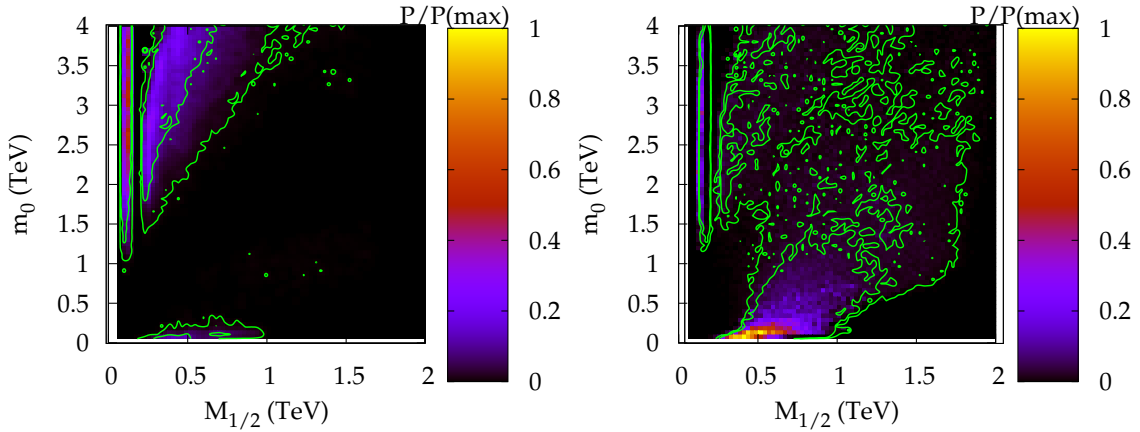


Figure 2: Posterior probability distributions in the $m_0 - m_{1/2}$ plane, taking into account the empirical inputs described in the text and using a natural prior (left) and a flat $\tan\beta$ prior (right), as described in the text. If naturalness considerations are taken into account, small $m_{1/2}$ and large m_0 are favored. In each frame, contours enclosing the 68% and 95% confidence regions are shown.

and $m_{1/2}$).

The shape of the posterior is dominated by the relic density constraint: the CMSSM tends to give much too high values for $\Omega_\chi h^2$ in generic parts of parameter space unless there exists a specific mechanism through which efficient annihilation

can occur. On the left-hand side of Figs. 1 and 2 (natural priors), we see that this results in a large posterior for the focus point region of parameter space, where there is a significant higgsino fraction in the composition of the lightest neutralino, causing it to efficiently annihilate into fermion and/or gauge boson pairs. There also exists a favored region in which $2m_{\chi_1^0} \approx m_{h^0}$ at the lowest values of $m_{1/2}$, disconnected from the other region. In this case, annihilation occurs through the lightest CP-even Higgs resonance into b and τ pairs.

On the right-hand side of Figs. 1 and 2, we show for comparison the results found using the flat $\tan\beta$ prior. For low values of $\tan\beta$, we have a vertical funnel on the right hand side of Fig. 1, corresponding to the stau co-annihilation region, where staus efficiently annihilate with the neutralino lightest SUSY particle (LSP) because of quasi mass degeneracy. At high $\tan\beta$, but moderate values of m_0 and $m_{1/2}$, $2m_{\chi_1^0} \sim m_{A^0}$, leading to efficient dark matter annihilation through s -channel pseudo-scalar Higgs boson exchange, into b and τ pairs. At low $m_{1/2}$, we again have the h^0 -pole annihilation region but, for flat $\tan\beta$ priors, small values of $\tan\beta$ are disfavored as they lead to values of m_{h^0} which are below the LEP2 limit. The LEP2 Higgs mass constraint also means that the h^0 region is outside the 68% contour. At high m_0 , the focus point is also in evidence for flat $\tan\beta$ priors.

Some features of the posterior distribution become much clearer when marginalized to one CMSSM parameter dimension. Such marginalizations are shown in Fig. 3, one for each of the four continuous CMSSM parameters. Three key differences are immediately noticed when comparing the results found using the natural and flat priors. Firstly, in considerable contrast to the flat $\tan\beta$ case, the natural prior strongly favors heavy sfermion masses (large m_0). Secondly, the natural prior prefers low to moderate values of $\tan\beta$, again in contrast to the flat $\tan\beta$ case. The posterior pdfs of m_0 and $\tan\beta$ therefore display themselves to be strongly prior dependent, whereas $m_{1/2}$ shows a smaller difference between the fits using the two priors, and A_0 shows very little dependence. Thus, the choice of theoretical prejudice alters the results of the fit for $\tan\beta$ and m_0 . The natural prior prefers somewhat smaller values of $m_{1/2}$ relative to those found using the flat prior. From the $m_{1/2}$ figure, we see the strong bi-modality of the posterior, where the spike at low values of $m_{1/2}$ corresponds to the h^0 -pole region.

Although one might expect values of m_0 much larger than M_Z^{emp} to require an unacceptable degree of fine tuning, this does not have to be the case. In particular, although large values of m_0 lead to large values of $\bar{m}_{H_{1,2}}^2$ unless counter-balanced by an almost equally large value of μ^2 in order to obtain the empirical value of $M_Z^{emp} = (91 \text{ GeV})^2$, this fine tuning can be avoided in portions of supersymmetric parameter space known as the focus point region (also known as the ‘hyperbolic branch’). In this region, the RG trajectories of the Higgs mass parameters meet at a point near the weak scale, at which their (small) values are independent of their input values at the UV boundary. This leads to a Higgs potential which is largely

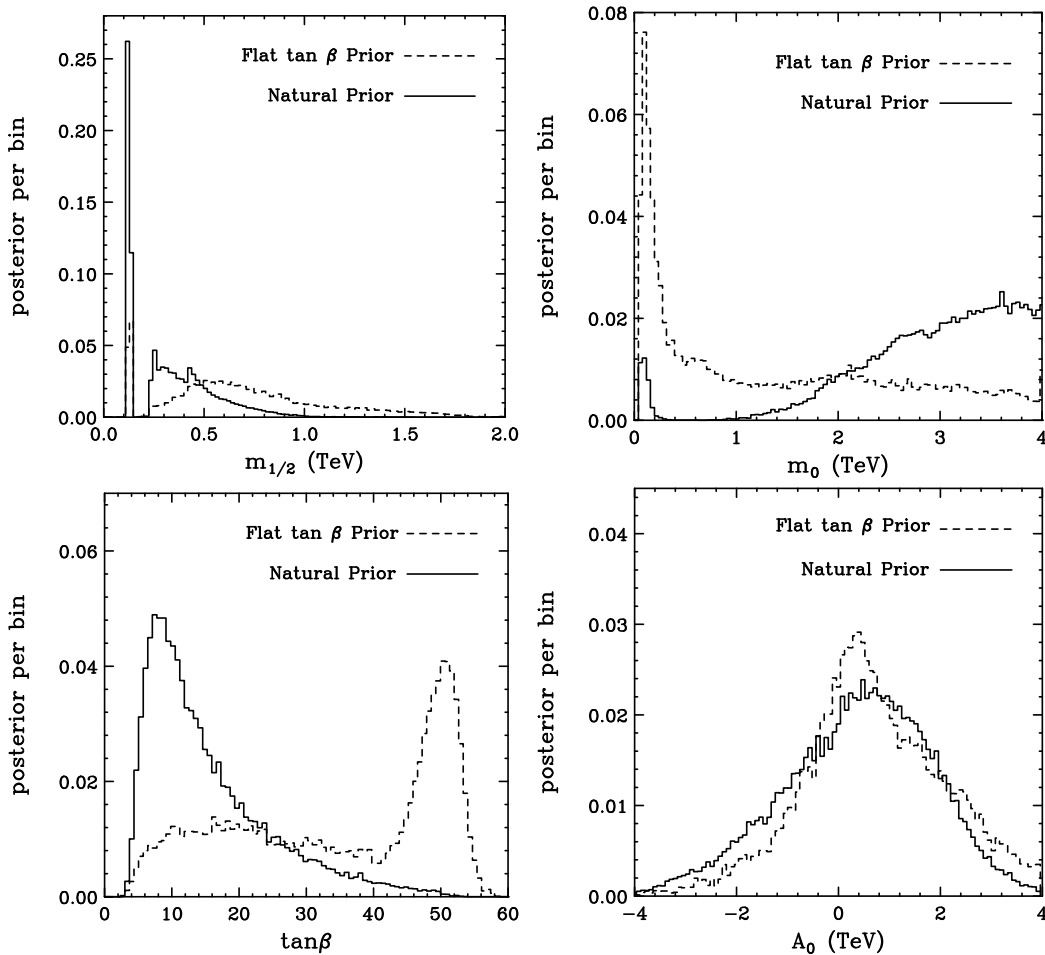


Figure 3: Posterior probability distributions of the CMSSM parameters, marginalized over the unseen parameters, taking into account the empirical inputs described in the text and using a flat $\tan\beta$ prior (dashed) or a natural prior (solid) as described in the text. For the natural measure, small to moderate values of $m_{1/2}$ and $\tan\beta$ are preferred, while m_0 is strongly favored to be large. In each frame, each distribution is plotted in 100 bins of equal width.

insensitive to the scalar masses. As a result, models with multi-TeV squarks, sleptons and heavy Higgs scalars can exist with only a modest degree of fine tuning [44].

Eq. 2.7 indicates that the natural prior favors lower $\tan\beta$ (thus suppressing the A^0 pole region) and low values of μ , which occur in the focus point region. We can see evidence of the latter by examining Fig. 4, where the logarithm of the marginal prior probability density is plotted as a function of m_0 and $\tan\beta$ for a scan where all data was ignored. μ is particularly low in the focus point region, and so the prior factor $1/\mu$ is the dominant factor in enhancing the focus point at high m_0 . We also see the preference for lower values of $\tan\beta$ in the figure evident in Eq. 2.7. Ref. [18] assumed significantly smaller theoretical errors on the prediction for the branching ratio of

$b \rightarrow s\gamma$ than ours. There, it was found that the current best-predicted value of the branching ratio from the Standard Model (found by including some higher order contributions in the calculation), additional preference for the focus point region was found compared to the case where the higher order contributions were neglected. If we were to reduce our assumed theoretical errors on the prediction of this quantity, we would obtain a similar further enhancement of the focus point region.

A very distinctive dark matter phenomenology emerges in the majority of the CMSSM parameter space favored by the natural prior. In particular, most of this space contains a rather light neutralino, with a mixed gaugino-higgsino composition as predicted by comparably low values of μ and $M_{1/2}$. Such mixed neutralinos, which appear in the focus point region, have

sizable couplings to SM gauge bosons and fermions which enable them to annihilate efficiently and avoid

being overproduced in the early universe. There also exists a sizable probability (approximately 35%), however, for the parameter space in which the lightest neutralino falls in the h^0 -pole region, without a large degree of higgsino composition. This region can be seen in the figures, and appears at $m_{1/2} \sim 100$ GeV or $m_{\chi^0} \approx 60$ GeV.

Writing the lightest neutralino as a mixture of gauginos (bino and wino) and higgsinos:

$$\chi^0 = N_{11}\tilde{B} + N_{12}\tilde{W}^3 + N_{13}\tilde{H}_1 + N_{14}\tilde{H}_2, \quad (3.1)$$

we define the gaugino and higgsino fractions as $|N_{11}|^2 + |N_{12}|^2$ and $|N_{13}|^2 + |N_{14}|^2$, respectively. Within the CMSSM, the assumption that the gaugino masses unify at a common scale ensures that $|N_{12}|^2$ is never much larger than a few percent. The relative bino and higgsino fractions of the lightest neutralino are, therefore, largely dictated by the ratio of M_1 (determined by $m_{1/2}$) and μ . In Fig. 5, we show the posterior probability distributions for the mass and higgsino fraction of the lightest neutralino. Interestingly, the natural priors lead to a strong preference for a highly mixed higgsino-bino composition for the lightest neutralino ($|N_{13}|^2 + |N_{14}|^2 \sim 0.1$). This is a direct consequence of being in the focus point region of supersymmetric parameter space. In particular, as m_0 is increased, the value of $|\mu|$, as determined by the electroweak symmetry breaking conditions, is driven to smaller values, thus increasing the higgsino content of the lightest neutralino. In the following sections we will explore the phenomenology and detection prospects for neutralino dark matter

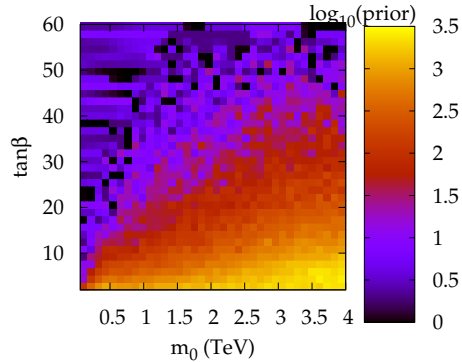


Figure 4: Marginalised natural prior as a function of m_0 and $\tan\beta$.

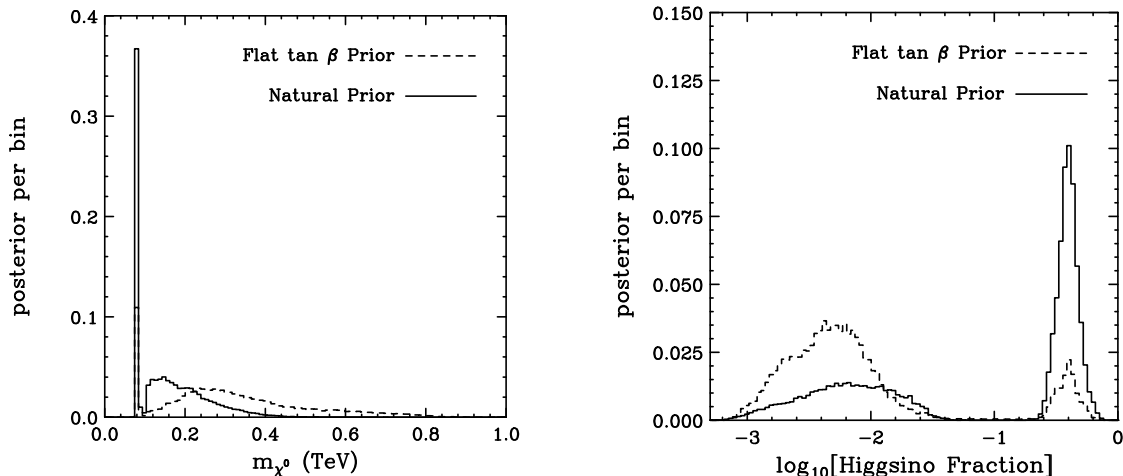


Figure 5: Posterior probability distributions for the mass of the lightest neutralino and its higgsino fraction, using a natural prior (solid) or a flat $\tan\beta$ prior (dashed), as described in the text. If naturalness considerations are taken into account, a light neutralino with a mixed higgsino-gaugino composition is favored. In each frame, each distribution is plotted in 100 bins of equal width.

with these properties.

4. Direct Detection

Searches for dark matter which attempt to detect such particles through their elastic scattering with nuclei are known as direct detection. Experiments currently involved in this effort include CDMS [45], XENON [46], ZEPLIN [47], Edelweiss [48], CRESST [49], WARP [50], KIMS [51], and COUPP [52].

The ability of experiments such as these to detect a weakly interacting massive particle (WIMP) depend on its mass and on its elastic scattering cross section with the nuclei making up the detector. The elastic scattering cross section of a neutralino or other WIMP can be broken into spin-independent and spin-dependent contributions. Spin-independent interactions represent coherent scattering with the entire nucleus, and lead to a cross section proportional to the square of the target nucleus' mass. Spin dependent interactions, in contrast, lead to a cross section that scales with $J(J+1)$, where J is the total spin of the target nucleus. Currently, direct constraints on spin-independent scattering are far more stringent than those for spin-dependent scattering. For this reason, we focus on spin-independent scattering in this section.

The spin-independent neutralino-nucleus elastic scattering cross section is given by:

$$\sigma \approx \frac{4m_{\chi^0}^2 m_T^2}{\pi(m_{\chi^0} + m_T)^2} [Zf_p + (A-Z)f_n]^2, \quad (4.1)$$

where m_T is the mass of the target nucleus, and Z , A are the atomic number and atomic mass of the nucleus, respectively. f_p and f_n are the neutralino's couplings to protons and neutrons, given by [53]:

$$f_{p,n} = \sum_{q=u,d,s} f_{T_q}^{(p,n)} a_q \frac{m_{p,n}}{m_q} + \frac{2}{27} f_{TG}^{(p,n)} \sum_{q=c,b,t} a_q \frac{m_{p,n}}{m_q}, \quad (4.2)$$

where a_q are the neutralino-quark couplings [53, 54] and $f_{T_q}^{(p,n)}$ denote the quark content of the nucleon and have been measured to be: $f_{T_u}^{(p)} \approx 0.020 \pm 0.004$, $f_{T_d}^{(p)} \approx 0.026 \pm 0.005$, $f_{T_s}^{(p)} \approx 0.118 \pm 0.062$, $f_{T_u}^{(n)} \approx 0.014 \pm 0.003$, $f_{T_d}^{(n)} \approx 0.036 \pm 0.008$ and $f_{T_s}^{(n)} \approx 0.118 \pm 0.062$ [55]. The first term in this equation corresponds to interactions with the quarks in the target, which can occur through either t -channel CP-even Higgs exchange, or s -channel squark exchange. The second term corresponds to interactions with gluons in the target through a quark/squark loop. $f_{TG}^{(p)}$ is given by $1 - f_{T_u}^{(p)} - f_{T_d}^{(p)} - f_{T_s}^{(p)} \approx 0.84$, and analogously, $f_{TG}^{(n)} \approx 0.83$.

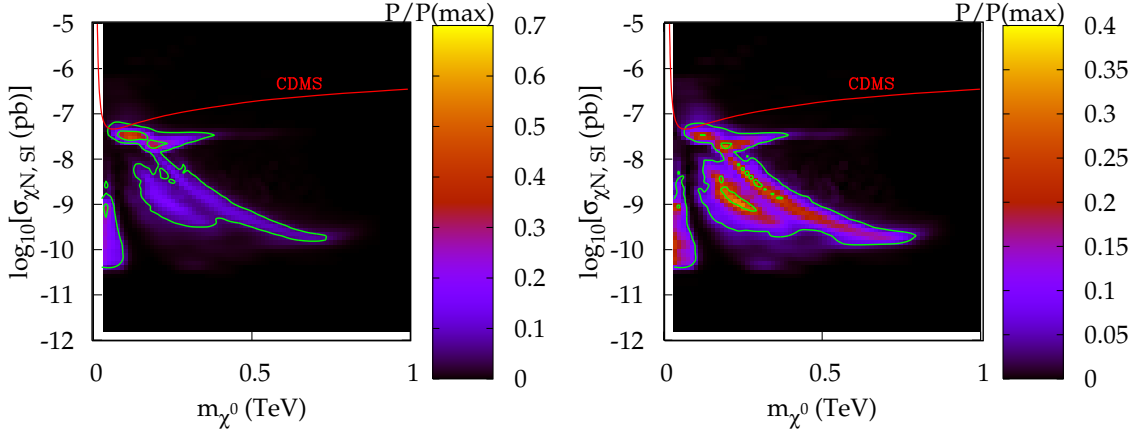


Figure 6: Posterior probability distributions in the neutralino-nucleon, spin-independent elastic scattering cross section vs neutralino mass plane, taking into account the empirical inputs and using the natural (left) and flat $\tan\beta$ (right) priors described in the text. If natural priors are used, the focus point region is preferred, leading to $\sigma_{\chi N,SI} \sim 3 \times 10^{-8}$ pb. The light Higgs pole region is also seen in the left frame with $m_{\chi^0} \sim 60$ GeV and a smaller cross section. In each frame, contours enclosing the 68% and 95% confidence regions are shown. Also shown is the 90% confidence level current upper bound placed by the CDMS collaboration [45] assuming a local dark matter density of $\rho_{\chi^0} = 0.3$ GeV/cm³ and a characteristic velocity of $v_0 = 230$ km/s.

In Fig. 6, we show the posterior probability distributions for the neutralino's spin-independent elastic scattering cross section (per nucleon), for the case of a natural prior (left) and a flat $\tan\beta$ prior (right). From this figure, it is clear that the most

probable parameter regions, corresponding to a highly mixed neutralino in the focus point, are concentrated around $\sigma_{\chi N, SI} \sim 3 \times 10^{-8}$ pb, which is just beyond the current reach of direct detection experiments such as CDMS [45]. It is straightforward to see why is the case. In the focus point region of the CMSSM, the squarks and heavy Higgs boson masses are large enough to not contribute significantly to the process of neutralino elastic scattering. In this case, and for a neutralino with a negligible wino content, the coupling a_q is proportional to $N_{11}N_{14}/m_h^2$. With the higgsino fraction predicted to be ~ 0.1 (as seen in the left frame of Fig. 5), the resulting elastic scattering cross section is expected to be quite large, leading to the results found in the left frame of Fig. 6. The lower left portion of the left hand frame of Fig. 6 corresponds to the light Higgs pole region, in which the lightest neutralino is largely bino-like. In this region, the neutralino-quark couplings and corresponding cross sections with nuclei are smaller compared to the mixed bino-higgsino region. In the right hand frame, we show the flat $\tan\beta$ prior direct detection cross section posterior probability for comparison. Despite our updated constraints and additional observables, the flat $\tan\beta$ posterior looks indistinguishable to the eye to previous determinations [17, 18], where the connection between a preference for the focus point and good direct detection prospects were pointed out.

Before moving on to the prospects for indirect detection, a few comments are in order. Firstly, direct detection experiments do not simply measure the WIMP's interaction cross section, but instead measure the cross section multiplied by the flux of WIMPs passing through the detector. The observed rate, therefore, depends on the local density of dark matter and, to a lesser degree, on its velocity distribution. Constraints such as those from CDMS shown in Fig. 6 are made under reasonable assumptions about the local dark matter density and velocity distribution. Measurements of the Milky Way's rotation curves can be used to estimate a local dark matter density in the range of 0.22 to 0.73 GeV/cm³ [56]. As long as the fine-grained structure of the dark matter distribution is not highly clumpy, this range should be appropriate for the purposes of direct detection (for discussions, see Ref. [57].) The nuclear physics involved in neutralino-nuclei scattering also introduces a degree of uncertainty into the constraints placed by direct detection experiments (for more details, see Ref. [58]).

5. Indirect Detection

5.1 Neutrino Telescopes

Through elastic scattering with nuclei in the Sun, neutralinos can become gravitationally bound, leading them to accumulate and annihilate in the Sun's core. Such annihilations can potentially produce a flux of high energy neutrinos observable to next generation neutrino telescopes [7].

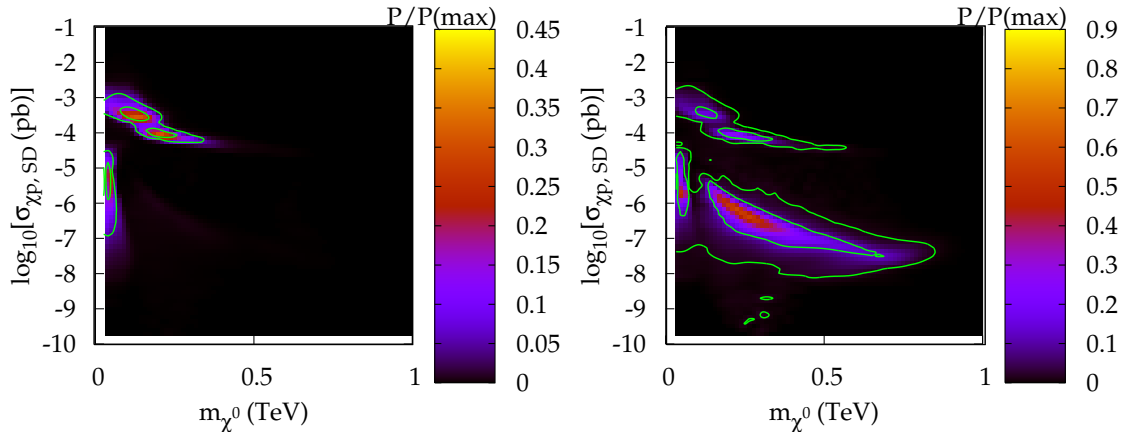


Figure 7: Posterior probability distributions in the neutralino-proton, spin-dependent elastic scattering cross section vs neutralino mass plane, taking into account the empirical inputs and using the natural (left) and flat $\tan\beta$ (right) priors described in the text. If naturalness considerations are taken into account, the focus point region is preferred, leading to $\sigma_{\chi^0 p, SD} \sim 10^{-4}$ pb. The light Higgs pole region is also seen in the left frame with $m_{\chi^0} \sim 60$ GeV and a smaller cross section. In each frame, contours enclosing the 68% and 95% confidence regions are shown.

Assuming a standard local density and velocity distribution, neutralinos become captured by the Sun at a rate given by [59]:

$$C^\odot \approx 3.35 \times 10^{19} \text{ s}^{-1} \left(\frac{\sigma_{\chi^0 p, SD} + \sigma_{\chi^0 p, SI} + 0.07 \sigma_{\chi^0 \text{He}, SI}}{10^{-7} \text{ pb}} \right) \left(\frac{100 \text{ GeV}}{m_{\chi^0}} \right)^2, \quad (5.1)$$

where $\sigma_{\chi^0 p, SD}$, $\sigma_{\chi^0 p, SI}$ and $\sigma_{\chi^0 \text{He}, SI}$ are the spin dependent (SD) and spin independent (SI) elastic scattering cross sections of neutralinos with hydrogen (protons) and helium nuclei, respectively. The factor of 0.07 reflects the solar abundance of helium relative to hydrogen and well as dynamical factors and form factor suppression.

In the previous section, we calculated the posterior probability for the neutralino's spin-independent elastic scattering cross section. In Fig. 7, we show the analogous result for the spin-dependent, neutralino-proton elastic scattering cross section. Again, we find that the natural priors lead to a strong preference for large elastic scattering cross sections. In this case, this results from the sizable higgsino couplings to the Z -boson, which leads to a cross section which scales as: $\sigma_{\chi^0 p, SD} \propto [|N_{13}|^2 - |N_{14}|^2]^2$. By comparing Figs. 6 and 7, we clearly see that the spin-dependent cross section will dominate the overall capture rate of neutralinos in the Sun. The flat $\tan\beta$ prior frame on the right hand side looks rather similar to the posterior obtained recently in the literature [18], despite the fact that it has been obtained with updated data and additional observables.

If the capture rate and annihilation cross section are sufficiently large, equilibrium will be reached between these processes. For a number of neutralinos in the Sun, N , the rate of change of this quantity is given by:

$$\dot{N} = C^\odot - A^\odot N^2, \quad (5.2)$$

where C^\odot is the capture rate and A^\odot is the annihilation cross section times the relative neutralino velocity per unit volume. The present neutralino annihilation rate in the Sun is given by:

$$\Gamma = \frac{1}{2} A^\odot N^2 = \frac{1}{2} C^\odot \tanh^2 \left(\sqrt{C^\odot A^\odot} t_\odot \right) \quad (5.3)$$

where $t_\odot \approx 4.5$ billion years is the age of the solar system. The annihilation rate is maximized when it reaches equilibrium with the capture rate (*ie.* when $\sqrt{C^\odot A^\odot} t_\odot \gg 1$). For the vast majority of the favored parameter space, we find that this condition is easily satisfied.

Neutralinos can generate neutrinos through a wide range of annihilation channels. Annihilations to heavy quarks, tau leptons, gauge bosons and Higgs bosons can each generate neutrinos in their subsequent fragmentation and decay. The muon neutrino spectrum at the Earth from neutralino annihilations in the Sun is given by:

$$\frac{dN_{\nu_\mu}}{dE_{\nu_\mu}} = \frac{C_\odot F_{\text{Eq}}}{4\pi D_{\text{ES}}^2} \left(\frac{dN_\nu}{dE_\nu} \right)^{\text{Inj}}, \quad (5.4)$$

where C_\odot is the capture rate of neutralinos in the Sun, F_{Eq} is the non-equilibrium suppression factor (≈ 1 for capture-annihilation equilibrium), D_{ES} is the Earth-Sun distance and $\left(\frac{dN_\nu}{dE_\nu} \right)^{\text{Inj}}$ is the neutrino spectrum from the Sun per neutralino annihilating. Due to $\nu_\mu - \nu_\tau$ vacuum oscillations, the muon neutrino flux observed at Earth is the average of the ν_μ and ν_τ components.

Muon neutrinos produce muons in charged current interactions with nuclei in the material inside or near the detector volume of a high energy neutrino telescope. The rate of neutrino-induced muons observed in a high-energy neutrino telescope is given by:

$$N_{\text{events}} \approx \int \int \frac{dN_{\nu_\mu}}{dE_{\nu_\mu}} \frac{d\sigma_\nu}{dy}(E_{\nu_\mu}, y) R_\mu((1-y) E_\nu) A_{\text{eff}} dE_{\nu_\mu} dy, \quad (5.5)$$

where $\sigma_\nu(E_{\nu_\mu})$ is the neutrino-nucleon charged current interaction cross section, $(1-y)$ is the fraction of neutrino energy which goes into the muon and A_{eff} is the effective area of the detector. R_μ is either the distance a muon of energy, $E_\mu = (1-y) E_\nu$, travels before falling below the muon energy threshold of the experiment, called the muon range, or the width of the detector, whichever is larger. The spectrum and flux of neutrinos generated in neutralino annihilations is determined by its mass and dominant annihilation modes.

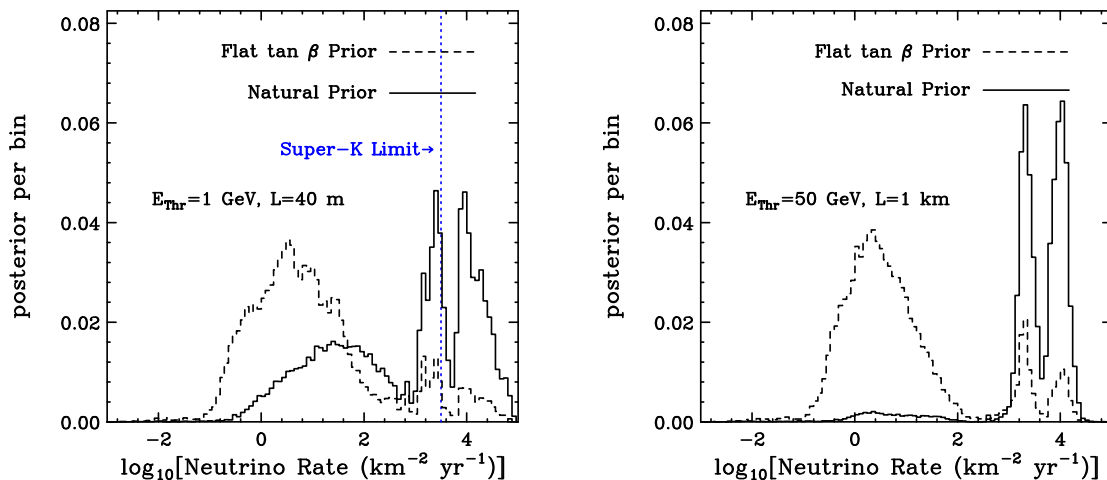


Figure 8: Posterior probability distributions for the rate of neutrino events from neutralino annihilations in the Sun (per square kilometer, per year), using a flat $\tan\beta$ prior (dashed) or a natural prior (solid) as described in the text. The left (right) frame corresponds to the rate predicted at the Super-Kamiokande (IceCube) experiment. In each frame, each distribution is plotted in 100 bins of equal width. Note that in the right frame, 39% of the distribution (the union of the light Higgs-pole region and the stau co-annihilation region) does not appear, as no events above the 50 GeV threshold are generated.

In Fig. 8, we show the posterior probability distribution for the rate of neutrino induced muons from dark matter annihilations in the Sun in a experiment such as Super-Kamiokande (left) [60] and in a kilometer-scale, high energy neutrino telescope such as IceCube (right) [61]. For Super-Kamiokande, we plot the rate of muons with an energy greater than 1 GeV, and use a detector width of 40 meters. For the case of IceCube, we have used a 50 GeV muon energy threshold, and a kilometer width.

Currently, the strongest constraint on the neutrino flux from dark matter annihilations in the Sun comes from Super-Kamiokande, which has placed an upper limit on the rate of neutrino-induced muons from the Sun of approximately 3×10^3 per square kilometer, per year [60]. Slightly weaker constraints have also been placed by Amanda [62], Baksan [63] and Macro [64]. The approximate Super-Kamiokande constraint is shown as a vertical dotted line in the left frame of Fig. 8. Assuming an average local dark matter density of 0.3 GeV/cm^3 , this bound excludes a sizable fraction (38%) of the probability distribution favored by our analysis. If a rather conservative value of 0.1 GeV/cm^3 were used instead, only 22% of the of the probability distribution is excluded by the Super-Kamiokande limit.

The predicted rates in IceCube, as shown in the right frame of Fig. 8, are extremely promising. About 61% of the probability distribution corresponds to models which would produce thousands of muon induced neutrino events per year from dark matter annihilations in the Sun. In contrast, the rate of atmospheric neutrino induced muons in the same angular window is only approximately 500 events per square

kilometer per year. Therefore, on the order of only $5 \times \sqrt{500} \sim 100$ events per square kilometer, per year would be required to produce a 5σ detection in IceCube.

The 35% of the probability distribution that falls in the light Higgs-pole region cannot be easily observed by IceCube, however, as these models contain neutralinos with ≈ 60 GeV masses, well below the range required to generate muons above IceCube’s energy threshold.

5.2 Gamma-Rays and Charged Particles

Dark matter annihilating throughout the Milky Way’s halo can potentially lead to observable fluxes of gamma-rays, electrons/positrons, antiprotons and/or antideuterons. The strategies for detecting gamma-rays from dark matter annihilation are quite different from those for charged particle searches, as gamma-rays travel undeflected by magnetic fields, making the observation of point-like or extended regions of high dark matter density possible. Some of the most promising regions include the center of the Milky Way [65] and nearby dwarf satellite galaxies [66]. Charged particles produced in dark matter annihilations, in contrast, diffuse in the galactic magnetic field erasing any directional information. Nonetheless, if the rate of dark matter annihilation is large enough in the galactic halo, it may be possible to identify its contribution in the antimatter component of the cosmic ray spectrum. Additionally, electrons and positrons produced through dark matter annihilations could potentially produce an observable flux of synchrotron radiation as they travelling through the Galactic Magnetic Fields [11].

The prospects for detecting dark matter with gamma-rays and charged particles each depend on both particle physics and astrophysical inputs. Regarding particle physics, the neutralino’s annihilation cross section and mass (and to a lesser extent its dominant annihilation modes) each impact the reach of indirect detection efforts. In Fig. 9, we show the posterior probability distribution for the annihilation cross section and mass of the lightest neutralino. Using natural priors, the favored focus point region leads to a cross section times relative velocity of $\sigma_{\text{Ann}}v \approx 3 \times 10^{-26}$ cm³/s, which is approximately the maximal value possible for a thermal WIMP. The models in the light Higgs-pole region have considerably smaller annihilation cross section, making their indirect detection with gamma-rays or charged cosmic rays very unlikely. If flat $\tan\beta$ priors are used, the neutralino’s annihilation cross section can be considerably smaller than the bulk of the favored natural prior region.

A number of astrophysical inputs also impact the reach of gamma-ray, cosmic ray and synchrotron searches for dark matter annihilation. In the case of gamma-rays and synchrotron radiation, the annihilation rate in the inner galaxy or elsewhere depends on the integral of the dark matter density squared, over the observed line-of-sight. This leads to a strong dependence on the density of dark matter in the inner parsecs of halos, well beyond the resolution of current N-body simulations. Furthermore, the gravitational potential in the inner region of the Milky Way is dominated by baryons

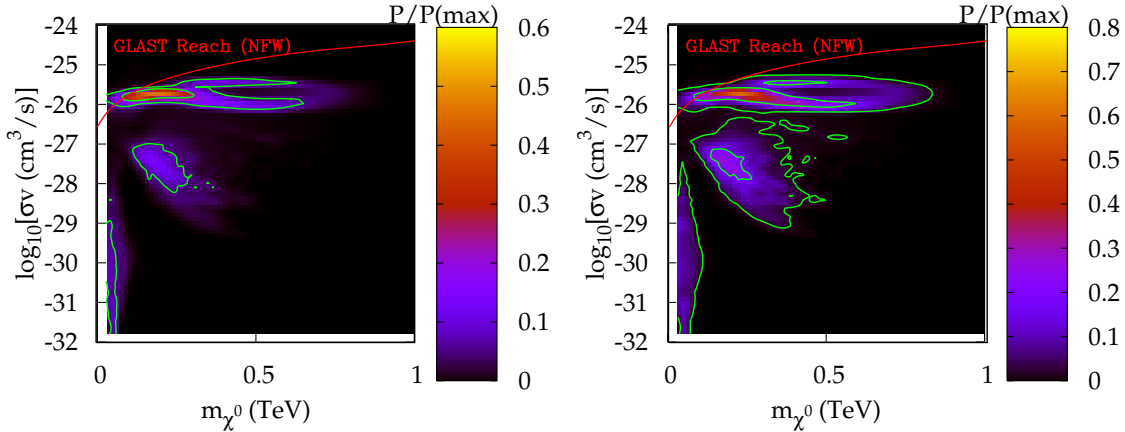


Figure 9: Posterior probability distributions in the annihilation cross section vs lightest neutralino mass plane, taking into account the empirical inputs and using the natural (left) and flat $\tan\beta$ (right) priors described in the text. If naturalness considerations are taken into account, the focus point region is preferred, leading to $\sigma_{\text{Ann}}v \sim 3 \times 10^{-26} \text{ cm}^3/\text{s}$. The light Higgs pole region is also seen in the left frame with $m_{\chi^0} \sim 60 \text{ GeV}$ and a smaller cross section times relative velocity. In each frame, contours enclosing the 68% and 95% confidence regions are shown. Also shown is the reach of the GLAST telescope for the case of a Navarro, Frenk and White (NFW), halo profile [67].

rather than dark matter, whose effects are not generally included in such simulations. Although the impact of baryonic matter on the dark matter distribution is difficult to predict, an enhancement in the dark matter density and corresponding annihilation rate is expected to result from the process of adiabatic compression [68]. The adiabatic accretion of dark matter onto the central super-massive black hole might also lead to the formation of a density spike in the dark matter distribution, leading to an enhanced dark matter annihilation rate [69]. Collectively, these astrophysical uncertainties lead to several orders of magnitude of variation in predictions of the gamma-ray flux from dark matter annihilations.

In Fig. 9, we show the projected reach of the GLAST gamma-ray telescope [70] after ten years of observation, as calculated in Ref. [67], for the case of a dark matter distribution following the Navarro, Frenk and White (NFW) profile [71], neglecting adiabatic compression and any other such effects. For this choice of the dark matter distribution, a non-negligible fraction of the posterior probability distribution favored by the natural priors are within GLAST’s reach. One again, we remind the reader that variations from the NFW profile could modify this projection considerably. If the dark matter annihilation rate is even mildly enhanced from that predicted for a simple NFW profile, GLAST could potentially probe the entire range of CMSSM parameter space favored by the natural priors. This is in contrast to the results found

using flat $\tan\beta$ priors, which allow for neutralinos with much smaller annihilation cross sections (see also Ref. [19]). We also note that, if the lightest neutralino is heavier than a few hundred GeV, ground-based atmospheric Cerenkov telescopes could also be used to search for dark matter annihilations in the inner Milky Way and elsewhere [72].

The prospects for the detection of cosmic ray electrons/positrons, antiprotons and antideuterons are also subject to large degree of astrophysical uncertainty. Namely, the diffusion parameters that describe the magnetic and radiation fields of the Milky Way [73], as well as the dark matter distribution, can significantly impact the reach of experiments such as PAMELA [74] and AMS-02 [75] to detect the presence of dark matter annihilations. In particular, the “boost factor” that results from inhomogeneities in the dark matter distribution can impact the prospects for such experiments considerably. For moderate choices of the diffusion parameters and boost factor (~ 1 -10), prospects for PAMELA to detect positrons from dark matter annihilations over the background of cosmic ray secondaries are similar to those for GLAST to detect gamma-rays [76], as shown in Fig. 9.

6. Summary and Conclusions

By considering measurements of quantities such as the anomalous magnetic moment of the muon, the $b \rightarrow s\gamma$ branching fraction, the $B_s \rightarrow \mu^+\mu^-$ branching fraction, the mass of the W boson, the effective leptonic mixing angle, Higgs boson and sparticle search constraints, and the cosmological dark matter abundance, it is possible to constrain the parameter space of supersymmetry. The results of global fits to such indirect data currently depend, however, on the choice of priors which are adopted. In most of the global fits of supersymmetric parameter space which have been performed to date, priors have been used which are flat in the derived quantity, $\tan\beta$. A far more natural choice would be to use priors which are flat (or perhaps, logarithmic) in the fundamental parameters μ and B . In this article, we have considered the impact of adopting such natural priors upon fits of the CMSSM to indirect data, focusing on the phenomenology of neutralino dark matter that is found in the parameter space favored by such fits.

Using natural priors and updated indirect data, we find that two regions of the CMSSM parameter space are strongly favored. Firstly, about 61% of the posterior probability distribution corresponds to the focus point region. Of the remainder, 35% of the posterior probability distribution corresponds to the light Higgs-pole region in which the lightest neutralino annihilates on resonance with the light Higgs boson and 4% corresponds to the stau co-annihilation region, where staus and other sleptons efficiently annihilate with the lightest neutralinos. In contrast to the results found using priors flat in $\tan\beta$, we find that the stau-co-annihilation and A -funnel regions

of the CMSSM parameter space contribute negligibly to the posterior probability distribution.

In the favored focus point region, the lightest neutralino is a mixed gaugino-higgsino ($\sim 10\%$ higgsino fraction) with a mass less than approximately 300 GeV. Such a neutralino has a very distinctive dark matter phenomenology and is nearly optimally suited for the purposes of direct and indirect detection. In particular, a mixed gaugino-higgsino neutralino possesses large couplings to Standard Model fermions, and thus has large elastic scattering cross sections with nuclei. In the light Higgs-pole region, the lightest neutralino can have considerably smaller couplings.

We find that neutralinos in the favored focus point region have a spin-independent elastic scattering cross section with nucleons of $\sim 3 \times 10^{-8}$ pb, which is within a factor of 2 (5) of the current limit from CDMS for a 100 GeV (300 GeV) neutralino. We, therefore, expect direct detection experiments to probe the majority of the posterior probability distribution of the CMSSM parameter space in the very near future.

The prospects for neutrino telescopes found using natural priors are also very promising. In particular, most of the favored parameter space predicts thousands of events to be observed per year in a kilometer-scale neutrino telescope such as IceCube. Current constraints from Super-Kamiokande already exclude 38% of the posterior probability distribution, assuming a local dark matter density of 0.3 GeV/cm^3 .

Although searches for dark matter using gamma-rays and charged particles depend strongly on unknown astrophysical inputs, our analysis finds that the majority of the favored parameter space predicts a neutralino annihilation cross section near the maximum possible for a thermal relic ($\sim 3 \times 10^{-26} \text{ cm}^3/\text{s}$). This along with the relatively light mass range favored for the lightest neutralino makes the prospects for GLAST and PAMELA to detect neutralino dark matter near optimal.

We believe that a prior that is flat in μ, B is a much more natural choice than one flat in $\tan\beta$. If the naturalness prior were complemented with an additional hyperparameter prior that enforces that all soft terms are “of the same order” [16], the focus point is *disfavoured*. However one can consider differences in the derived posterior probability distributions from the different priors as evidence that more data is needed to constrain the model. Thus, fit predictions that are robust (i.e. approximately invariant) with respect to changes in assumed prior distributions are not attained for mSUGRA, since it has many parameters and the data constraining it are rather indirect. While this is undeniably true, it is still interesting to examine the effect of the more natural prior as it gives us our “best bet” for quantities such as the dark matter-nucleon cross-sections relevant for direct detection, or galactic annihilation cross sections relevant for indirect detection. Our neutralino-nucleon cross-sections coming from the fit for the flat $\tan\beta$ prior are similar to other previous determinations in the literature, providing validation of our calculations. Our best guess for this quantity leads to a good chance that a further increase of a factor of 10 in sensitivity by the experiments will lead to a direct detection discovery. Had,

instead of priors flat in μ, B , we had chosen priors that are flat in $\log \mu$ and $\log B$, we expect that our fits would show even stronger preference for the focus point: an additional factor of $1/(\mu B)$ in the integrand of Eq. 2.7 would have led to even more preference for the focus point region, with an associated extra boost in detection cross-sections.

Taken together, the results presented in this article are very encouraging for the prospects for direct and indirect efforts to detect neutralino dark matter. If natural choices are made in constructing priors, fits to the currently available data predict that, within the context of the CMSSM, the lightest neutralino is likely to have large elastic scattering and annihilation cross sections. In particular, the majority of the posterior probability distribution of the CMSSM parameter space (about 61%) should be within the reach of very near future direct detection experiments, and should be detectable in the near future by IceCube.

Voltaire’s satirical philosopher Pangloss long held the position that we live in the “best of all possible worlds”. We find that if naturalness considerations are taken into account, then (modulo the usual astrophysical uncertainties) the prospects for the direct and indirect detection of neutralino dark matter in the CMSSM are, if not Panglossian, are at least extremely encouraging.

Acknowledgments

DH is supported by the Fermi Research Alliance, LLC under Contract No. DE-AC02-07CH11359 with the US Department of Energy and by NASA grant NNX08AH34G. This work has been partially supported by STFC. The computational work has been performed using the Cambridge eScience CAMGRID computing facility, with the invaluable help of M. Calleja.

References

- [1] For a review of supersymmetry phenomenology, see: S. P. Martin, arXiv:hep-ph/9709356.
- [2] J. R. Ellis, S. Kelley and D. V. Nanopoulos, Phys. Lett. B **260**, 131 (1991).
- [3] H. Goldberg, Phys. Rev. Lett. **50**, 1419 (1983); J. R. Ellis, J. S. Hagelin, D. V. Nanopoulos, K. A. Olive and M. Srednicki, Nucl. Phys. B **238**, 453 (1984).
- [4] E. Komatsu *et al.*, [arXiv:0803.0547].
- [5] G. Bertone, D. Hooper and J. Silk, Phys. Rept. **405**, 279 (2005) [arXiv:hep-ph/0404175].
- [6] L. Bergstrom, P. Ullio and J. H. Buckley, Astropart. Phys. **9**, 137 (1998) [arXiv:astro-ph/9712318]; L. Bergstrom, J. Edsjo and P. Ullio, Phys. Rev. Lett. **87**,

- 251301 (2001) [arXiv:astro-ph/0105048]; V. Berezhinsky, A. Bottino and G. Mignola, Phys. Lett. B **325**, 136 (1994) [arXiv:hep-ph/9402215].
- [7] L. Bergstrom, J. Edsjo and P. Gondolo, Phys. Rev. D **55**, 1765 (1997) [arXiv:hep-ph/9607237]; Phys. Rev. D **58**, 103519 (1998) [arXiv:hep-ph/9806293]; F. Halzen and D. Hooper, Phys. Rev. D **73**, 123507 (2006) [arXiv:hep-ph/0510048]; V. D. Barger, F. Halzen, D. Hooper and C. Kao, Phys. Rev. D **65**, 075022 (2002).
- [8] E. A. Baltz and J. Edsjo, Phys. Rev. D **59** (1999) 023511 [arXiv:astro-ph/9808243]; S. Profumo and P. Ullio, JCAP **0407**, 006 (2004) [arXiv:hep-ph/0406018].
- [9] L. Bergstrom, J. Edsjo and P. Ullio, arXiv:astro-ph/9906034; A. Bottino, F. Donato, N. Fornengo and P. Salati, Phys. Rev. D **58**, 123503 (1998); F. Donato, N. Fornengo, D. Maurin, P. Salati and R. Taillet, arXiv:astro-ph/0306207.
- [10] F. Donato, N. Fornengo and P. Salati, Phys. Rev. D **62**, 043003 (2000) [arXiv:hep-ph/9904481]; H. Baer and S. Profumo, JCAP **0512**, 008 (2005) [arXiv:astro-ph/0510722].
- [11] E. A. Baltz and L. Wai, Phys. Rev. D **70**, 023512 (2004) [arXiv:astro-ph/0403528]; M. P. Blasi, A. V. Olinto and C. Tyler, Astropart. Phys. **18**, 649 (2003) [arXiv:astro-ph/0202049]; D. P. Finkbeiner, arXiv:astro-ph/0409027; S. Colafrancesco, S. Profumo and P. Ullio, Astron. Astrophys. **455**, 21 (2006) [arXiv:astro-ph/0507575]; L. Bergstrom, M. Fairbairn and L. Pieri, Phys. Rev. D **74**, 123515 (2006) [arXiv:astro-ph/0607327]. D. Hooper, D. P. Finkbeiner and G. Dobler, Phys. Rev. D **76**, 083012 (2007), arXiv:0705.3655 [astro-ph].
- [12] J. R. Ellis, S. Heinemeyer, K. A. Olive and G. Weiglein, JHEP **0605**, 005 (2006) [arXiv:hep-ph/0602220]; J. R. Ellis, K. A. Olive and V. C. Spanos, Phys. Lett. B **624**, 47 (2005) [arXiv:hep-ph/0504196]; J. R. Ellis, S. Heinemeyer, K. A. Olive and G. Weiglein, JHEP **0502**, 013 (2005) [arXiv:hep-ph/0411216]; J. R. Ellis, S. Heinemeyer, K. A. Olive, A. M. Weber and G. Weiglein, JHEP **0708**, 083 (2007) [arXiv:0706.0652 [hep-ph]]; J. R. Ellis, K. A. Olive, Y. Santoso and V. C. Spanos, Phys. Rev. D **69** (2004) 095004 [arXiv:hep-ph/0310356].
- [13] S. Profumo and C. E. Yaguna, Phys. Rev. D **70** (2004) 095004 [arXiv:hep-ph/0407036].
- [14] B. C. Allanach and C. G. Lester, Phys. Rev. D **73**, 015013 (2006) [arXiv:hep-ph/0507283].
- [15] L. Roszkowski, R. R. de Austri and R. Trotta, JHEP **0704** (2007) 084 [arXiv:hep-ph/0611173].
- [16] B. C. Allanach, K. Cranmer, C. G. Lester and A. M. Weber, JHEP **0708**, 023 (2007) [arXiv:0705.0487 [hep-ph]].

- [17] R. R. de Austri, R. Trotta and L. Roszkowski, *JHEP* **0605** (2006) 002 [arXiv:hep-ph/0602028].
- [18] L. Roszkowski, R. Ruiz de Austri and R. Trotta, *JHEP* **0707**, 075 (2007) [arXiv:0705.2012 [hep-ph]].
- [19] L. Roszkowski, R. R. de Austri, J. Silk and R. Trotta, arXiv:0707.0622 [astro-ph].
- [20] D. M. Pierce, J. A. Bagger, K. T. Matchev and R.-J. Zhang, *Nucl. Phys. B* **491** (1997) 3, [arXiv:hep-ph/9606211].
- [21] B.C. Allanach, *Comput. Phys. Commun.* **143** (2002) 305, [arXiv:hep-ph/0104145].
- [22] W. -M. Yao et al. [Particle Data Group], *J. Phys.* **G33** (2006) 1. and 2007 partial update for 2008.
- [23] B. C. Allanach, C. G. Lester and A. M. Weber, *JHEP* **12** (2006) 065 [arXiv:hep-ph/0609295]
- [24] B. C. Allanach, *Phys. Lett. B* **635**, 123 (2006) [arXiv:hep-ph/0601089].
- [25] R. Barbieri and G. F. Giudice, *Nucl. Phys. B* **306** (1988) 63; B. de Carlos and J. A. Casas, *Phys. Lett. B* **309** (1993) 320, [arXiv:hep-ph/9303291]; R. Barbieri and A. Strumia, *Phys. Lett. B* **433** (1998) 63, [arXiv:hep-ph/9801353]; C. Giusti, A. Romanano and A. Strumia. *Nucl. Phys. B* **550**, 3 (1999) [arXiv:hep-ph/9811386]; L. E. Ibanez and G. G. Ross, arXiv:hep-ph/0702046.
- [26] [CDF Collaboration and D0 Collaboration], arXiv:0803.1683 [hep-ex].
- [27] available at <http://www.slac.stanford.edu/xorg/hfag/rare/lep-pho07/radll/index.html>
- [28] F. Mahmoudi, *JHEP* **12** (2007) 026 [arXiv:0710.3791].
- [29] UTfit Collaboration, *JHEP* (2006) [hep-ph/0606167].
- [30] K. Hagiwara, A.D. Martin, D. Nomura, and T. Teubner, (2006) [arXiv:hep-ph/0611102].
- [31] Tevatron Electroweak Working Group & The CDF Collaboration, *Winter 2007 Conference Note*, <http://fcdwww.fnal.gov/physics/ewk/2007/wmass/>.
- [32] [The ALEPH, DELPHI, L3 and OPAL Collaborations, the LEP Electroweak Working Group], arXiv:0712.0929.
- [33] Precision Electroweak Measurements and Constraints on the Standard Model, The LEP Collaboration, arXiv:0712.0929.
- [34] P. Gambino, U. Haisch and M. Misiak, *Phys. Rev. Lett.* **94** (2005) 061803 [arXiv:hep-ph/0410155].

- [35] P. Skands *et al.*, JHEP **0407** (2004) 036, [arXiv:hep-ph/0311123].
- [36] G. Blanger, F. Boudjema, A. Pukhov, A. Semenov, arXiv:0803.2360 [hep-ph]; G. Blanger, F. Boudjema, A. Pukhov, A. Semenov, Comput.Phys.Commun.176:367-382,2007 hep-ph/0607059; G. Bélanger, F. Boudjema, A. Pukhov and A. Semenov, Comput. Phys. Commun. **174** (2006) 577 [arXiv:hep-ph/0405253]; G. Bélanger, F. Boudjema, A. Pukhov and A. Semenov, Comput. Phys. Commun. **149** (2002) 103 [arXiv:hep-ph/0112278].
- [37] G.W. Bennett *et al.* [Muon g-2 collaboration], Phys. Rev. D **73** (2006) 072003 [arXiv:hep-ex/0602035].
- [38] F. Mahmoudi Computer Physics Communications (2008), [arXiv:0710.2067].
- [39] The code is forthcoming in a publication by A. M. Weber *et al.*; S. Heinemeyer, W. Hollik, D. Stöckinger, A. M. Weber and G. Weiglein, JHEP **08** (2006) 052, [arXiv:hep-ph/0604147].
- [40] A. J. Buras, P. H. Chankowski, J. Rosiek and L. Slawianowska, Nucl. Phys. B **659**, 3 (2003) [arXiv:hep-ph/0210145].
- [41] G. Isidori and P. Paradisi, Phys. Lett. B **639**, 499 (2006) [arXiv:hep-ph/0605012].
- [42] B. C. Allanach and C. G. Lester, arXiv:0705.0486 [hep-ph]
- [43] A. Gelman and D. Rubin, *Inference from Iterative Simulation Using Multiple Sequences*, Stat. Sci. **7** (1992) 457.
- [44] K. L. Chan, U. Chattopadhyay and P. Nath, Phys. Rev. D **58**, 096004 (1998) [arXiv:hep-ph/9710473]; J. L. Feng, K. T. Matchev and T. Moroi, Phys. Rev. Lett. **84**, 2322 (2000) [arXiv:hep-ph/9908309]; J. L. Feng, K. T. Matchev and T. Moroi, Phys. Rev. D **61**, 075005 (2000) [arXiv:hep-ph/9909334]; J. L. Feng, K. T. Matchev and T. Moroi, arXiv:hep-ph/0003138; D. Feldman, Z. Liu and P. Nath, Phys. Lett. B **662**, 190 (2008) [arXiv:0711.4591 [hep-ph]].
- [45] Z. Ahmed *et al.* [CDMS Collaboration], arXiv:0802.3530 [astro-ph].
- [46] J. Angle *et al.* [XENON Collaboration], arXiv:0706.0039 [astro-ph].
- [47] G. J. Alner *et al.*, Astropart. Phys. **28**, 287 (2007) [arXiv:astro-ph/0701858]; G. J. Alner *et al.* [UK Dark Matter Collaboration], Astropart. Phys. **23**, 444 (2005).
- [48] V. Sanglard *et al.* [The EDELWEISS Collaboration], Phys. Rev. D **71**, 122002 (2005) [arXiv:astro-ph/0503265].
- [49] G. Angloher *et al.*, Astropart. Phys. **23**, 325 (2005) [arXiv:astro-ph/0408006].
- [50] P. Benetti *et al.*, arXiv:astro-ph/0701286; R. Brunetti *et al.*, New Astron. Rev. **49**, 265 (2005) [arXiv:astro-ph/0405342].

- [51] H. S. Lee. *et al.* [KIMS Collaboration], Phys. Rev. Lett. **99**, 091301 (2007) [arXiv:0704.0423 [astro-ph]].
- [52] W. J. Bolte *et al.*, J. Phys. Conf. Ser. **39**, 126 (2006).
- [53] G. Jungman, M. Kamionkowski and K. Griest, Phys. Rept. **267**, 195 (1996) [arXiv:hep-ph/9506380].
- [54] G. B. Gelmini, P. Gondolo and E. Roulet, Nucl. Phys. B **351**, 623 (1991); M. Srednicki and R. Watkins, Phys. Lett. B **225**, 140 (1989); M. Drees and M. Nojiri, Phys. Rev. D **48**, 3483 (1993) [arXiv:hep-ph/9307208]; M. Drees and M. M. Nojiri, Phys. Rev. D **47**, 4226 (1993) [arXiv:hep-ph/9210272]; J. R. Ellis, A. Ferstl and K. A. Olive, Phys. Lett. B **481**, (2000) 304, [arXiv:hep-ph/0001005].
- [55] A. Bottino, F. Donato, N. Fornengo and S. Scopel, Astropart. Phys. **18**, 205 (2002) [arXiv:hep-ph/0111229]; Astropart. Phys. **13**, 215 (2000) [arXiv:hep-ph/9909228]; J. R. Ellis, K. A. Olive, Y. Santoso and V. C. Spanos, Phys. Rev. D **71**, 095007 (2005) [arXiv:hep-ph/0502001].
- [56] E. I. Gates, G. Gyuk and M. S. Turner, Phys. Rev. D **53** (1996) 4138 [arXiv:astro-ph/9508071], E. Gates, G. Gyuk and M. S. Turner, arXiv:astro-ph/9704253.
- [57] A. Helmi, S. D. M. White and V. Springel, Phys. Rev. D **66**, 063502 (2002) [arXiv:astro-ph/0201289]; M. Vogelsberger, S. D. M. White, A. Helmi and V. Springel, arXiv:0711.1105 [astro-ph].
- [58] A. E. Nelson and D. B. Kaplan, Phys. Lett. B **192**, 193 (1987); D. B. Kaplan and A. Manohar, Nucl. Phys. B **310**, 527 (1988); A. Bottino, F. Donato, N. Fornengo and S. Scopel, Astropart. Phys. **18**, 205 (2002) [arXiv:hep-ph/0111229]; J. R. Ellis, K. A. Olive, Y. Santoso and V. C. Spanos, Phys. Rev. D **71**, 095007 (2005) [arXiv:hep-ph/0502001].
- [59] A. Gould, Astrophys. J. **388**, 338 (1991).
- [60] S. Desai *et al.* [Super-Kamiokande Collaboration], Phys. Rev. D **70**, 083523 (2004) [Erratum-ibid. D **70**, 109901 (2004)] [arXiv:hep-ex/0404025].
- [61] T. DeYoung [IceCube Collaboration], Int. J. Mod. Phys. A **20**, 3160 (2005); J. Ahrens *et al.* [The IceCube Collaboration], Nucl. Phys. Proc. Suppl. **118**, 388 (2003) [arXiv:astro-ph/0209556].
- [62] M. Ackermann *et al.* [AMANDA Collaboration], arXiv:astro-ph/0508518; See also the new preliminary results described in the talk by T. De Young at *Neutrino 08, the XXIII International Conference on Neutrino Physics and Astrophysics*, Christchurch, New Zealand (2008).

- [63] M. M. Boliev *et al.*, Proc. of the Intl. Workshop on Aspects of Dark Matter in Astrophysics and Particle Physics, Heidelberg, Germany, 1996. Edited by H. V. Klapdor-Kleingrothaus, Y. Ramachers. Singapore, World Scientific, 1997.
- [64] M. Ambrosio *et al.* [MACRO Collaboration], Phys. Rev. D **60**, 082002 (1999) [arXiv:hep-ex/9812020].
- [65] A. Cesarini, F. Fucito, A. Lionetto, A. Morselli and P. Ullio, Astropart. Phys. **21**, 267 (2004) [arXiv:astro-ph/0305075]; P. Ullio, L. Bergstrom, J. Edsjo and C. G. Lacey, Phys. Rev. D **66**, 123502 (2002) [arXiv:astro-ph/0207125]; G. Zaharijas and D. Hooper, Phys. Rev. D **73**, 103501 (2006) [arXiv:astro-ph/0603540].
- [66] N. W. Evans, F. Ferrer and S. Sarkar, Phys. Rev. D **69**, 123501 (2004) [arXiv:astro-ph/0311145]; L. Bergstrom and D. Hooper, Phys. Rev. D **73**, 063510 (2006) [arXiv:hep-ph/0512317]; L. E. Strigari, S. M. Koushiappas, J. S. Bullock, M. Kaplinghat, J. D. Simon, M. Geha and B. Willman, arXiv:0709.1510 [astro-ph].
- [67] S. Dodelson, D. Hooper and P. D. Serpico, arXiv:0711.4621 [astro-ph].
- [68] F. Prada, A. Klypin, J. Flix, M. Martinez and E. Simonneau, arXiv:astro-ph/0401512; G. Bertone and D. Merritt, Mod. Phys. Lett. A **20**, 1021 (2005) [arXiv:astro-ph/0504422].
- [69] P. Gondolo and J. Silk, Phys. Rev. Lett. **83**, 1719 (1999) [arXiv:astro-ph/9906391]; P. Ullio, H. Zhao and M. Kamionkowski, Phys. Rev. D **64**, 043504 (2001) [arXiv:astro-ph/0101481]; G. Bertone, G. Sigl and J. Silk, Mon. Not. Roy. Astron. Soc. **337**, 98 (2002) [arXiv:astro-ph/0203488].
- [70] N. Gehrels and P. Michelson, Astropart. Phys. **11**, 277 (1999); S. Peirani, R. Mohayaee and J. A. de Freitas Pacheco, Phys. Rev. D **70**, 043503 (2004) [arXiv:astro-ph/0401378].
- [71] J. F. Navarro, C. S. Frenk and S. D. M. White, Astrophys. J. **462**, 563 (1996) [arXiv:astro-ph/9508025]; J. F. Navarro, C. S. Frenk and S. D. M. White, Astrophys. J. **490**, 493 (1997).
- [72] F. Aharonian *et al.* [The HESS Collaboration], Astron. Astrophys. **425**, L13 (2004) [arXiv:astro-ph/0408145]; J. Albert *et al.* [MAGIC Collaboration], Astrophys. J. **638**, L101 (2006) [arXiv:astro-ph/0512469].
- [73] For a recent review, see: A. W. Strong, I. V. Moskalenko and V. S. Ptuskin, Ann. Rev. Nucl. Part. Sci. **57**, 285 (2007) [arXiv:astro-ph/0701517].
- [74] P. Picozza *et al.*, Astropart. Phys. **27**, 296 (2007) [arXiv:astro-ph/0608697].
- [75] M. Sapinski [AMS Collaboration], Acta Phys. Polon. B **37**, 1991 (2006); C. Goy [AMS Collaboration], J. Phys. Conf. Ser. **39**, 185 (2006).
- [76] D. Hooper and J. Silk, Phys. Rev. D **71**, 083503 (2005) [arXiv:hep-ph/0409104].